THE JOURNAL OF BIOLOGICAL CHEMISTRY VOL. 285, NO. 3, pp. 1587–1596, January 15, 2010

Metabolic Fluxes during Strong Carbon Catabolite Repression by Malate in *Bacillus subtilis*[*][S]

Received for publication, September 2, 2009, and in revised form, October 14, 2009 Published, JBC Papers in Press, November 16, 2009, DOI 10.1074/jbc.M109.061747

Roelco J. Kleijn[‡], Joerg M. Buescher[‡], Ludovic Le Chat[§], Matthieu Jules[§], Stephane Aymerich[§], and Uwe Sauer[‡1]

From the [‡]Institute of Molecular System Biology, ETH Zürich, CH-8093 Zürich, Switzerland and the [§]Institut National de la Recherche Agronomique (UMR1238), CNRS (UMR2585), and AgroParisTech, Microbiologie et Génétique Moléculaire, F-78850 Thiverval-Grignon, France

Commonly glucose is considered to be the only preferred substrate in *Bacillus subtilis* whose presence represses utilization of other alternative substrates. Because recent data indicate that malate might be an exception, we quantify here the carbon source utilization hierarchy. Based on physiology and transcriptional data during co-utilization experiments with eight carbon substrates, we demonstrate that malate is a second preferred carbon source for *B. subtilis*, which is rapidly co-utilized with glucose and strongly represses the uptake of alternative substrates. From the different hierarchy and degree of catabolite repression exerted by glucose and malate, we conclude that both substrates might act through different molecular mechanisms. To obtain a quantitative and functional network view of how malate is (co)metabolized, we developed a novel approach to metabolic flux analysis that avoids error-prone, intuitive, and ad hoc decisions on ^{13}C rearrangements. In particular, we developed a rigorous approach for deriving reaction reversibilities by combining *in vivo* intracellular metabolite concentrations with a thermodynamic feasibility analysis. The thus-obtained analytical model of metabolism was then used for network-wide isotopologue balancing to estimate the intracellular fluxes. These ^{13}C-flux data revealed an extraordinarily high malate influx that is primarily catabolized via the gluconeogenic reactions and toward overflow metabolism. Furthermore, a considerable NADPH-producing malic enzyme flux is required to supply the biosynthetically required NADPH in the presence of malate. Co-utilization of glucose and malate resulted in a synergistic decrease of the respiratory tricarboxylic acid cycle flux.

Typically, microbes prefer a single carbon source whose presence represses utilization of alternative substrates. The classical example is the diauxic shift of *Escherichia coli* with subsequent growth on first glucose and then lactose (1). This widespread phenomenon, referred to as carbon catabolite repression, has been intensively studied in many chemoorganotrophic microbes, and in the vast majority of documented cases, the preferred carbon source is glucose (2, 3). Apart from repressing the co-utilization of alternative substrates, preferred carbon sources are normally associated with a high specific growth rate and substantial secretion of overflow metabolites such as ethanol, lactate, or acetate. For the Gram-positive model bacterium *Bacillus subtilis*, glucose has long been recognized to be preferred, but recent data indicated that glucose might not be the only preferred carbon source (4, 5).

According to the current model of the global carbon catabolite repression mechanism in *B. subtilis*, glucose-induced catabolite repression is mediated by the HPr kinase-catalyzed phosphorylation of HPr at its Ser-46 residue (2). This effect is propagated throughout the cell by the pleiotropic transcription factor CcpA (6), whose binding to the target sites for catabolite repression is controlled by the presence of HPr(Ser-P). CcpA imposes a strict hierarchy on carbon source utilization, where carbohydrates transported via the phosphoenolpyruvate (PEP)[2]-dependent phosphotransferase system (PTS) are catabolized first followed by non-PTS carbohydrates and, last, by organic acids (3, 5, 7, 8).

Based on indirect evidence, the gluconeogenic organic acid malate is a possible exception to this hierarchy. Unlike many other carboxylic acids, malate is rapidly metabolized by *B. subtilis*, allowing for a similar doubling time as with glucose (4). Although for most gluconeogenic carbon sources such as citrate, succinate, and fumarate, catabolite repressor (cre) binding sites have been found upstream of the genes involved in their transport (5, 9), no such cre sites have been found upstream of the malate-Na^+ symporter encoding *maeN* gene (10). Moreover, expression of *dctP*, encoding the generic C_4-dicarboxylic transporter for succinate and fumarate, is repressed by the addition of malate (5). These observations raise the question of whether malate would also be a preferred carbon source for *B. subtilis.* By characterizing the physiology of growth on malate and through carbon source co-utilization studies, we present both physiological and transcriptional proof that this is indeed the case.

Given the preferential status of malate for *B. subtilis*, we became interested in how malate is metabolized. To obtain a quantitative and functional network view, we used ^{13}C-based flux analysis (11). The first prerequisite for an accurate estima-

* This work was supported by European Union BaSysBio Program Grant LSHG-CT-2006-037469.

[S] The on-line version of this article (available at http://www.jbc.org) contains supplemental Appendices A–C.

[1] To whom correspondence should be addressed: Institute of Molecular System Biology, ETH Zurich, Wolfgang-Pauli-Strasse 16, CH-8093 Zürich, Switzerland. Tel.: 41-44-633-3672; E-mail: sauer@imsb.biol.ethz.ch.

[2] The abbreviations used are: PEP, phosphoenolpyruvate; FBP, fructose 1,6-phosphate; PTS, phosphotransferase system; NET analysis, network-embedded thermodynamic analysis; $\Delta G'^{\circ}_{f}$, standard thermodynamic formation energy; $\Delta G'^{\circ}_{R}$, standard Gibbs energy of reaction; GFP, green fluorescent protein; TCA, tricarboxylic acid; PP, pentose phosphate; HPLC, high performance liquid chromatography; TOF, time-of-flight; GC, gas chromatography.

tion of fluxes from ^{13}C rearrangements is a correct stoichiometric network model with defined reaction reversibilities (12, 13). Although this knowledge is readily available for model organisms grown on glucose (14–16), one cannot simply extrapolate these reaction reversibilities to alternative growth conditions. To avoid error-prone, intuitive, and ad hoc decisions, we describe here a rigorous and generalized approach to derive these reaction reversibilities (see Fig. 1). The approach is based on determining quantitative metabolomic data under the considered conditions and combining these with predetermined standard thermodynamic formation energies ($\Delta G'^{o}_{f}$) of the reactants that are defined in the stoichiometric network model. The framework of network-embedded thermodynamic (NET) analysis (17, 18) is then used to calculate the actual Gibbs energies ($\Delta G'^{o}_{R}$) for all reactions in the network. These $\Delta G'^{o}_{R}$ values are directly related to the reversibilities of the reactions (19). Using this general framework, we derived substrate-specific network models for exponentially growth of *B. subtilis* on glucose, malate, and the mixture of glucose plus malate that were subsequently used to quantify intracellular fluxes from ^{13}C-labeling experiments.

EXPERIMENTAL PROCEDURES

Strain and Growth Conditions—All physiological and flux analysis experiments were performed with wild-type *B. subtilis* BSB168 *trp*+ (20). For each growth experiment, frozen glycerol stocks were used to inoculate 5 ml of Luria-Bertani (LB) medium. After 5 h of growth at 37 °C, LB cultures were used to inoculate 5 ml of M9 minimal medium precultures at dilutions ranging from 500- to 2000-fold. The range of dilutions was chosen to assure that M9 precultures reached an optical density at 600 nm (A_{600}) between 0.5 and 1.0 upon overnight incubation. The M9 medium precultures with an A_{600} between 0.5 and 1.0 were used to inoculate 30 ml of M9 medium in 500 ml of non-baffled shake flasks to a starting A_{600} of 0.03–0.05. Cultivation was done at 300 rpm and 37 °C in an orbital shaker with a shaking diameter of 50 mm.

The M9 minimal medium consisted of the following components (per liter): 8.5 g of $Na_2HPO_4{\cdot}2H_20$, 3 g of KH_2PO_4, 1 g of NH_4Cl, 0.5 g of NaCl. The following components were sterilized separately and then added (per liter of final medium): 1 ml of 0.1 M $CaCl_2{\cdot}2H_2O$, 1 ml of 1 M $MgSO_4{\cdot}7H_2O$, 1 ml of 50 mM $FeCl_3{\cdot}6H_2O$, and 10 ml of trace salt solution. The trace salts solution contained (per liter): 170 mg of $ZnCl_2$, 100 mg of $MnCl_2{\cdot}4H_2O$, 60.0 mg of $CoCl_2{\cdot}6H_2O$, 60.0 mg of $Na_2MoO_4{\cdot}2H_2O$, and 43.0 mg $CuCl_2{\cdot}2H_2O$. When preparing the medium, the base salts were added first followed by $CalCl_2$, $MgSO_4$, $FeCl_3$, and finally the trace elements. Filter-sterilized carbon sources were added separately to the medium at the final concentrations shown in Table 1. Where necessary, carbon source solutions were pH-neutralized with 4 M NaOH before filter-sterilization. For ^{13}C-labeling experiments, the same final concentrations were used, but the carbon source was added directly to the shake flask. Both D-glucose and L-malate were added as a mixture of 20% (wt/wt) uniformly labeled carbon source (both > 99% isotopic purity; Cambridge Isotope Laboratories, Andover, MA) and 80% (wt/wt) naturally labeled carbon source.

TABLE 1
Carbon source concentrations in the described growth experiments

Carbon source	Concentration[a]	
	Single carbon source	Dual carbon source
	g/liter	
D-Glucose	3	2
L-Malic acid	5	4
D-Fructose	3	2
Sodium D-gluconate	4	3
Sodium pyruvate	6	4
Glycerol	6	3
D-Arabinose	4	2
Fumaric acid	5	3
Succinic acid[b]	4	2

[a] Concentrations were chosen such that the total carbon molecular mol content of the medium remained approximately 200 mmol carbon/liter.
[b] In the absence of glucose, *B. subtilis* cultures grown on succinic acid are auxotrophic for glutamate (58). Consequently, 2g/liter glutamic acid was added to all cultures grown in the presence of succinic acid (both as single or dual carbon source).

Physiological Parameters—Extracellular substrate and byproduct concentrations were measured by HPLC analysis using an Agilent 1100 series HPLC stack (Agilent Technologies, Waldbronn, Germany) in combination with an Aminex HPX-87H polymer column (Bio-Rad). Sugars were detected with a refractive index detector, and organic acids were detected with a UV-visible detector. Specific rates were calculated by regression analysis for at least five time points during the exponential growth phase as described previously (21). Cell growth was monitored photometrically at 600 nm, and cell dry weight was inferred from a predetermined conversion factor of 0.48 g of cells/A_{600} (22). All physiological parameters were determined during the exponential growth phase, typically ranging from 0.10 to 1.5 A_{600}.

Expression Studies—Green fluorescent protein (GFP) reporter strains of *glpF* or *dctP* transcription were obtained by insertion of either a fragment containing the entire *glpF* regulatory region (from −271 to + 130 relative to the transcription start) or the 3′ end region of the *dctP* gene (from +866 to +1466 relative to the translation start) into the pBaSysBioII plasmid upstream of the promoter-less *gfpmut3* gene (23) and then inserting the resulting plasmids into BSB168 strain (20) chromosome by single crossing-over recombination.

Three independent clones were cultivated in 96-well plates into an incubator/reader (Synergy 2; Biotek, Winooski, VT) at 37 °C with shaking in the same media as those used for the uptake measurement experiments. Growth (A_{600}) and fluorescence (485/528 nm) were followed every 10 min. Each clone was cultivated in at least two independent wells for each tested condition, and each plate (one for succinate ± glucose or malate, one for glycerol ± glucose or malate) was replicated twice. The expression of each fusion was, thus, determined using at least eight different cultures in each studied condition. Growth rates were similar to those obtained in shake flasks.

The fluorescence signal was corrected for background using the fluorescence signal of the BSB168 strain (without the *gfpmut3* gene). The expression levels of both fusions were calculated as $dGFP/dt/A$ for 5 time points during the exponential phase (0.3–0.9 at A_{600}) of each independent culture.

Sampling and Extracting for Metabolite Quantification—Quenching of cell metabolism based on cold solvent mixtures was shown to result in unspecific metabolite leakage and is,

thus, not suitable for bacteria (24). Hence we used a rapid centrifugation method where 1 ml of culture broth was transferred into a 1.5-ml tube and centrifuged for 15 s at 14,000 × *g* in a tabletop centrifuge (Eppendorf, Hamburg, Germany). The supernatant was decanted, and the pellet was immediately frozen in liquid nitrogen. Metabolites were extracted from the pellets by the addition of 1 ml of extracting solution at 78 °C. Aliquots for intracellular metabolite quantification were taken in triplicate from the shake flask cultures during exponential growth at a A_{600} between 0.8 and 1.2.

The extraction solution consisted of 60% (v/v) ethanol buffered with 10 mM ammonium acetate at pH 7.2. Directly after the addition of the extraction solution, 5 nmol each of norvaline and glutarate were added as internal standards. Pellets were extracted three times for 1 min at 78 °C while shaking at 1000 rpm in a Thermomixer (Eppendorf). Extracts were cooled on ice until further centrifugation. The metabolite extract was separated from cell debris by centrifugation at 14,000 × *g* at 4 °C for 10 min. The supernatants were pooled and dried at 0.12 millibar to complete dryness in a SpeedVac setup composed of an Alpha 2–4 LD plus cooling trap, RVC 2-33 rotational vacuum concentrator, and RC-5 vacuum chemical hybrid pump (Christ, Osterode am Harz, Germany). Dry metabolite extracts were stored at −80 °C until analysis.

Analytical Platforms for Metabolite Quantification; GC-TOF Workflow—The GC-TOF workflow is described in detail by Ewald *et al.* (25). Dried aliquots were derivatized with 15 μl of either TMS-reagent (*N*-methyl-*N*-(trimethylsilyl)trifluoro acetamide, Fluka, Buchs, Switzerland) or TBDMS reagent (*N*-*tert*-butyldimethylsilyl-*N*-methyltrifluoroacetamide, Fluka), and aliquots of 5 μl were injected into a 30-m GC column (HP-5-MS, 30 m × 0.25 mm × 0.25 μm, Agilent) using a CIS4 injector (Gerstel, Mülheim an der Ruhr, Germany) and solvent venting. Derivatized metabolites were detected on a Pegasus 3D TOF mass spectrometer (Leco), with an acquisition rate of 40 Hz. Peak detection and assignment were performed with ChromaTOF software (Version 2.32, Leco).

Analytical Platforms for Metabolite Quantification; Liquid Chromatography-MS/MS Workflow—The ion-pairing liquid chromatography method is described in detail by Büscher *et al.* (26). Dry metabolite extracts were resuspended in 100 μl of water, 8 μl of which were injected on a Agilent 1100 series HPLC stack with a Synergi Hydro RP 2.1 × 150 × 4 column (Phenomenex, Aschaffenburg, Germany). Metabolites were detected using a 4000 QTRAP mass spectrometer (AB/MDS Sciex, Concord, Canada) operated in tandem MS mode with unit mass resolution. Analyst software (Version 1.4.2, AB/MDS Sciex) was used for both acquisition and integration. Ion spray voltage, auxiliary gas temperature, nebulizer gas, auxiliary gas, curtain gas, and collision gas were set to −4200 V, 650 °C, and 65, 40, 10, 4 (arbitrary units), respectively.

A General Thermodynamic Framework for Deriving Reaction Reversibilities—Thermodynamic feasibility of the acquired metabolite datasets were computationally verified by NET analysis (17). Using the MatLab-based software anNET (18), measured metabolite concentrations, published Gibbs standard energies of formation for physiological conditions (27), and a genome-scale stoichiometric network (28) were combined to derive feasible ranges for the Gibbs energies of reactions (min/max $\Delta G'_R$). The original model of 1020 metabolic reactions and 988 metabolites was reduced to a core model with 166 reactions and 147 metabolites by omitting all metabolites for which no thermodynamic data were available. The intracellular pH was set to be 7.8 (29), and the ionic strength was assumed to be 0.15 M (30).

Recently it was shown that the quotient of net and exchange fluxes are coupled to the Gibbs energies of enzyme reactions (19, 31). The exchange flux theorem defined by Wiechert (19) states that the forward and backward flux of a multistep reaction mechanism is directly correlated to the $\Delta G'_R$,

$$\rho_R \leq \frac{\overrightarrow{v}}{\overleftarrow{v}} \leq \rho \qquad \text{(Eq. 1)}$$

$$\rho = \exp\left(-\frac{\Delta G'_R}{RT}\right) \qquad \text{(Eq. 2)}$$

where ρ is the non-equilibrium coefficient of the overall mechanism, and ρ_R is the coefficient of the reaction steps of the mechanism. Typically, binding steps and state transformations in a multistep reaction mechanism are close to equilibrium; in practice it holds that the flux ratio is approximately equal to ρ, yielding

$$\frac{\overrightarrow{v}}{\overleftarrow{v}} \approx \exp\left(-\frac{\Delta G'_R}{RT}\right) \qquad \text{(Eq. 3)}$$

By combining this theorem with the Gibbs energies of reaction derived from NET analysis we obtain a rational approach for deriving reaction reversibilities (Fig. 1).

Here we adopt the criterion that a reaction is considered unidirectional if the value of the forward or the backward flux exceeds the other by at least 50 times. For ^{13}C-labeling experiments, this means that of every 50 ^{13}C molecules converted by the forward reaction, less than one ^{13}C molecule is converted by the backward reaction. For all practical purposes the contribution of the backward flux to the overall labeling distribution of the surrounding metabolites can be neglected in such cases. By combining this criterion with Equations 4 and 5 (see later in the section), four cases can be defined (Fig. 2).

If the minimal and maximum $\Delta G'_R$ for a reaction ranges between −10 and 10 kJ/mol, the reaction is defined as reversible. If both the minimal and maximum $\Delta G'_R$ for a reaction are smaller than −10 kJ/mol, the reaction is unidirectional, and the backward reaction is negligible. If both the minimal and maximum $\Delta G'_R$ for a reaction are larger than 10 kJ/mol, the reaction is unidirectional, and the forward reaction is negligible. If the minimal and maximum $\Delta G'_R$ span either −10 or 10 kJ/mol, the reaction reversibility is undefined and modeled as reversible. Consequently, no constraints are imposed on the feasible ^{13}C distributions.

Biomass Sampling and GC-MS Analysis—Biomass aliquots (30 ml ≈ 15 mg of biomass dry weight) for analyzing the ^{13}C-labeling pattern of the proteinogenic amino acids were harvested from shake flask cultures during exponential growth. To ensure isotopic steady state, biomass samples were harvested at

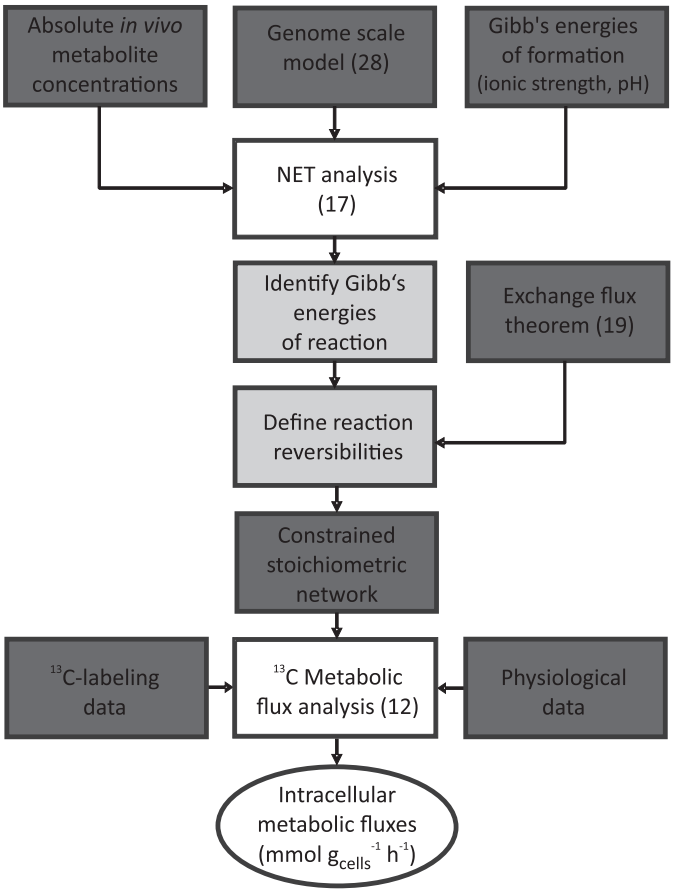

FIGURE 1. **Flow diagram for deriving intracellular metabolic fluxes using condition-specific metabolic network models.** Using NET analysis, intracellular metabolite concentrations were combined with thermodynamic data and network stoichiometry to calculate Gibbs energies of reactions. Using the exchange flux theorem (19), the Gibbs energies of reaction can be translated into reversibility constraints on the stoichiometric network. *Dark gray*, *light gray*, and *white rectangles* are inputs, actions, and tools, respectively. The *ellipse* indicates the output.

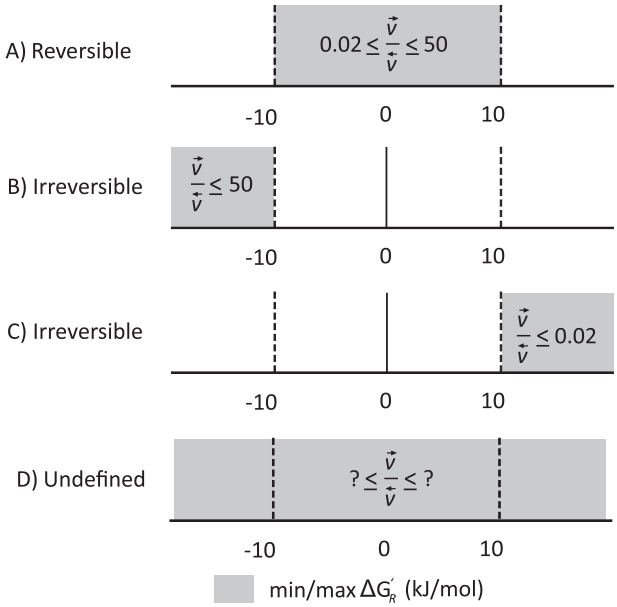

FIGURE 2. **Illustration of the four possible reversibility constraints imposed by the Gibbs energy of a reaction on the stoichiometric network for metabolic flux analysis.** The *gray area* denotes the range of feasible Gibbs energies of reaction. In this study we adopt the criterion that a reaction is unidirectional if either the forward or the backward flux is 50 times as big as the other.

an A_{600} of 1.0 ± 0.2 (13). The samples were centrifuged for 2 min at 10,000 × *g*, the supernatant was discarded, and the cell pellet was washed with 0.9% (w/v) NaCl solution. Aliquots of 5 mg of biomass were hydrolyzed in 1 ml of 6 M HCl, dried, and derivatized as described by Fischer and Sauer (32). In a next step GC-MS analysis and raw data analysis were performed (32). The obtained isotopologue fractions were corrected for the occurrence of natural isotopes of nitrogen, hydrogen, oxygen, sulfur, and silicon in both the amino acid and the derivatizing agent and for the occurrence of natural isotopes of C in the derivatizing agent only.

Stoichiometric Network Models—Stoichiometric network models were based on a core model containing the reactions of central carbon metabolism defined by Oh *et al.* (28). Feasible ranges for the $\Delta G'_R$ were obtained from anNET and combined with the exchange flux theorem of Wiechert (19) to classify the reaction in the stoichiometric network as either unidirectional forward, unidirectional backward, or reversible. By default, all reactions in the initial network were set to be reversible. Reversible reactions were modeled as separate forward and backward reactions and are referred to as net and exchange fluxes.

$$v_{net} = v_{forward} - v_{backward} \quad \text{(Eq. 4)}$$

$$v_{exchange} = \min(v_{forward}, v_{backward}) \quad \text{(Eq. 5)}$$

The growth rate-dependent biomass requirements of *B. subtilis* were previously established by Dauner *et al.* (16) and added to the network as unidirectional biomass precursor-withdrawing reactions. For a detailed overview of the reactions included into the stoichiometric network model, see supplemental Appendix A.

Metabolic Flux Analysis—Metabolic fluxes were derived using whole isotopologue analysis (15, 33). In short, the procedure uses the cumomer balances and cumomer to isotopologue mapping matrices introduced by Wiechert *et al.* (34) to calculate the isotopologue distributions of metabolites in a pre-defined stoichiometric network model for a given flux-set. The flux-set that gives the best correspondence between the measured and simulated ^{13}C-label distribution is determined by non-linear optimization and denoted as the optimal flux-fit. All calculations were performed in Matlab 7.6.0 (The Mathworks Inc., Natick, MA).

RESULTS

Physiology of Malate and Glucose Co-utilization in B. subtilis—Given previous indications of malate as a possible exception to the CcpA-imposed hierarchy of catabolite repression (4, 5, 9), we hypothesized that its utilization might not be repressed by glucose. To test this hypothesis, we first determined the culture physiology during growth on either glucose or malate and the mixture of both in minimal medium (Table 2). Consistent with previous data (4), virtually identical growth rates were observed on glucose and on malate, but malate was consumed at an unusual 4-fold higher specific rate. Most likely as a conse-

TABLE 2
Physiological parameters of *B. subtilis* 168 wild type during exponential growth on glucose, malate, and co-utilization of glucose plus malate

Substrate	Growth rate	Specific uptake rate		Specific production rate	
		Glucose	Malate	Pyruvate	Acetate
	h^{-1}	$mmol\ g^{-1}\ h^{-1}$		$mmol\ g^{-1}\ h^{-1}$	
Glucose	0.59 ± 0.02	7.63 ± 0.11		0.10 ± 0.03	3.79 ± 0.40
Malate	0.57 ± 0.05		26.51 ± 2.01	3.93 ± 0.14	9.50 ± 1.79
Glucose plus malate	0.75 ± 0.01	5.94 ± 1.09	14.60 ± 1.56	4.97 ± 0.60	7.16 ± 1.40

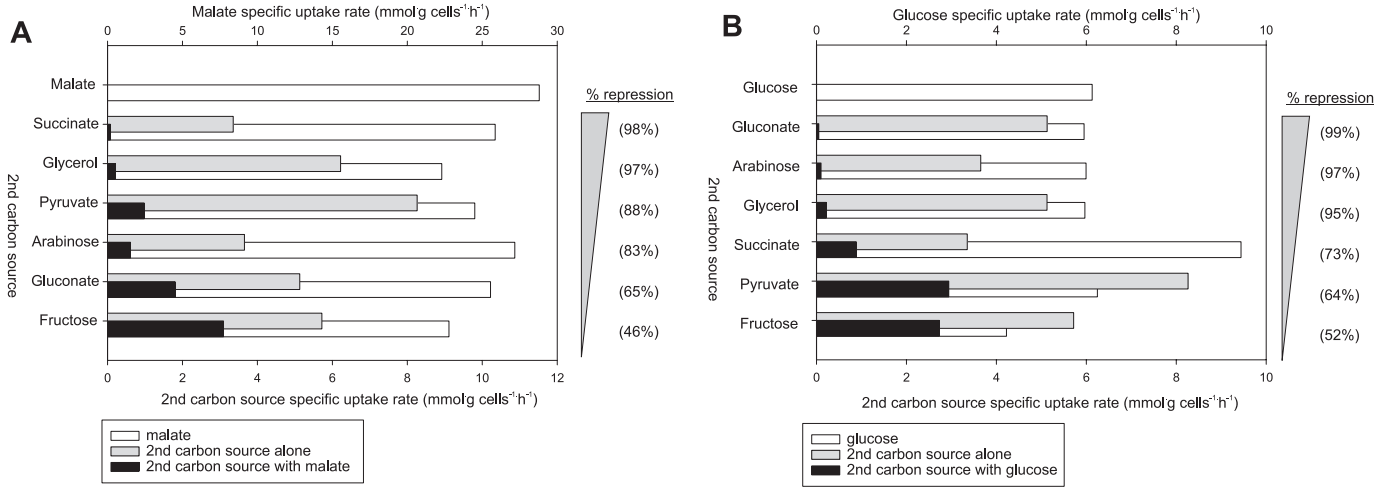

FIGURE 3. **Degree of physiological repression on the specific uptake rate of six alternative carbon sources by malate (*A*) and glucose (*B*) during exponential batch growth of *B. subtilis* 168 in minimal medium.** Specific uptake rates were determined both in the presence (*black bars*) and absence (*gray bars*) of malate and glucose to quantify the effect of co-utilization. The specific malate (*A*) and glucose (*B*) uptake rates are given in *white bars*.

quence of the high uptake rate, a higher fraction of the consumed carbon was secreted as overflow metabolites; *i.e.* 34% (mol/mol) on malate *versus* 15% on glucose. Moreover, pyruvate was the new main overflow product on malate, whereas only acetate was formed on glucose. Consistent with the above hypothesis, glucose and malate were fully co-utilized at a specific rate of growth that was higher than on the individual substrates. These physiological data, in particular the concomitant uptake of glucose and malate, demonstrate that malate does not comply with the previously proposed hierarchy in carbon source utilization for *B. subtilis* (3, 5, 7, 8).

Is malate uptake simply not repressed by glucose, or is malate itself a preferred substrate that exerts repression? To differentiate between these two possibilities, we designed malate co-utilization experiments in minimal medium batch culture with any one of six other carbon sources. In all cases malate was consumed at an almost unaltered high rate but reduced the uptake of the second substrate drastically to values between 54 and 2% that of the rate seen with the single carbon sources (Fig. 3*A*). Growth rates for the co-utilization experiments remained largely unchanged compared with growth on malate alone (data not shown). The least repressive effect of malate was observed for the PTS-sugar fructose, whose uptake rate was reduced by about 50%. In contrast, near complete repression was found for the tricarboxylic acid (TCA) cycle intermediate succinate and the two lower glycolytic substrates glycerol and pyruvate. With the exception of succinate and glycerol, all investigated carbon sources were still slowly co-utilized with malate, albeit at strongly reduced rates.

For a quantitative comparison of the repressive nature and strength of malate and glucose, we repeated the above co-utilization experiments with glucose instead of malate (Fig. 3*B*). Similar to malate, glucose was consumed at an almost unaltered rate while drastically repressing the uptake of the second carbon source to values ranging from 48 to 1% that of the rate seen with the single carbon source. Again, growth rates of the co-utilization experiments remained largely unchanged, with the exception of a slightly increased growth rate during co-utilization of succinate (data not shown). Nevertheless, the repressive effect of glucose on the measured uptake rates was more pronounced and exhibited a somewhat different repression hierarchy on the six carbon sources; *e.g.* a near complete repression arabinose, gluconate, and glycerol by glucose.

Malate and Glucose Transcriptionally Repress Genes Involved in Co-utilization—To verify the physiologically characterized repression by malate and glucose during co-utilization experiments at the transcriptional level, we constructed GFP transcriptional fusions for the glycerol and succinate uptake genes *glpF* and *dctP*, respectively. Glycerol and succinate are the most repressed carbon sources during co-utilization with malate, and both their uptake encoding genes are subject to glucose catabolite transcriptional repression via CcpA (35). During co-utilization experiments, both promoter activities were clearly repressed in the presence of either malate or glucose but at different degrees (Table 3). The transcriptional repression exerted by glucose on either the succinate (72%) or glycerol (100%) uptake promoters was virtually identical to the physiological repression of the uptake rates, 73 and

95%, respectively (Fig. 3*B*). Transcriptional repression of malate on the two promoters was, although strong, significantly less than the nearly complete physiological repression of succinate or glycerol uptake (Fig. 3*A*). Apparently, malate transcriptional repression alone does not suffice for complete uptake inhibition of the secondary carbon source, thereby indicating that further repressive mechanisms might be active.

Given that malate is concomitantly taken up with glucose and that both repress the uptake of alternative carbon sources at the transcriptional and physiological level, we conclude that malate and glucose are repressive and preferred carbon sources for *B. subtilis*. Because the degree and hierarchy of their repressive effects differ significantly both at the physiological and transcriptional level, we have first evidence that different molecular mechanisms underlie repression by either substrate.

TABLE 3

Transcriptional repression of succinate and glycerol uptake genes by glucose or malate

Transcriptional repression is represented in percentage ±S.E.

1st carbon source	Second carbon source	
	Succinate	Glycerol
Glucose	72 ± 6	100 ± 4
Malate	68 ± 7	51 ± 4

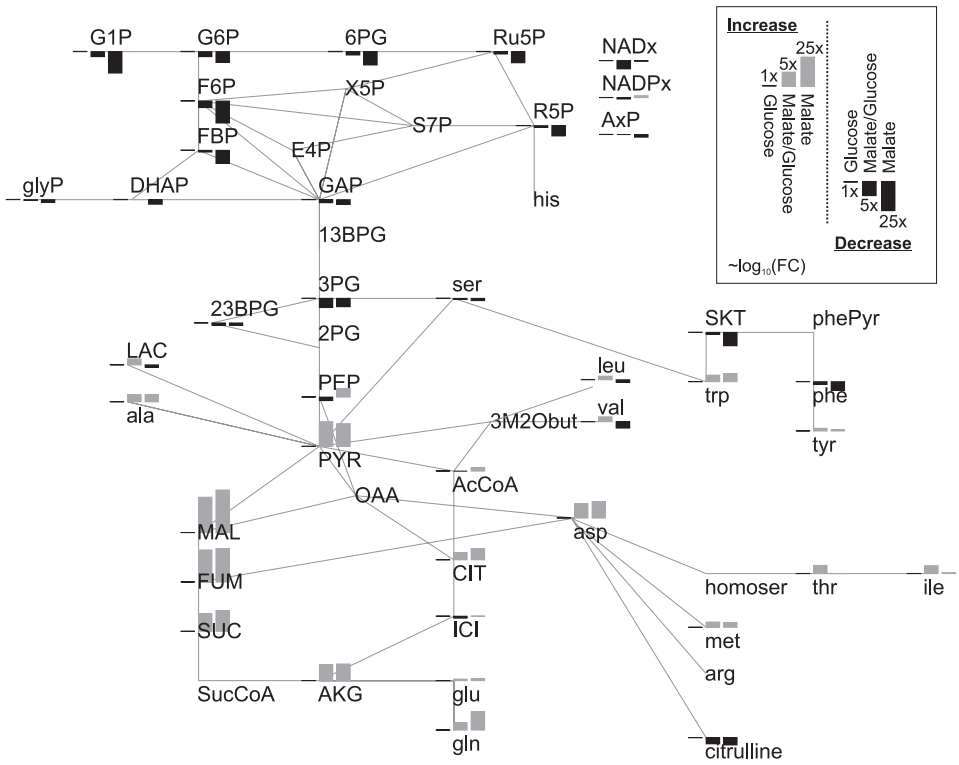

FIGURE 4. **-Fold changes in intracellular metabolite concentrations of *B. subtilis* 168 grown on malate and a mixture of glucose plus malate relative to the concentrations on glucose.** *Gray* and *black bars* denote a -fold drop and -fold increase, respectively. The data are from triplicate biological replicates and three technical replicates of each taken within 5 min during exponential growth. -Fold changes are scaled logarithmically, and the size of the -fold change is depicted by the height of the *bar*. The -fold changes were derived from the absolute concentrations and S.D. given in supplemental Appendix B. *BPG*, biphosphoglyceric acid; *PG*, phosphoglyceric acid; *AKG*, 2-oxoglutaric acid; *AxP*, combined pool of all adenosine phosphates; *CIT*, citrate; *DHAP*, dihydroxyacetone phosphate; *E4P*, erythrose-4-phosphate; *F6P*, fructose 6-phosphate; *FC*, fold-change; *FUM*, fumaric acid; *G1P*, glucose 1-phosphate; *G6P*, glucose 6-phosphate; *GAP*, glyceraldehyde 3-phosphate; *glyP*, glycerol monophosphate; *ICI*, isocitric acid; *LAC*, lactic acid; *MAL*, malic acid; *NADx*, combined pool of NADH and NAD; *NADPx*, combined pool of NADPH and NADP; *OAA*, oxaloacetate; *PEP*, phosphoenolpyruvic acid; *R5P*, ribose 5-phosphate; *Ru5P*, ribulose 5-phosphate; *S7P*, sedoheptulose 7-phosphate; *SKT*, shikimate; *X5P*, xylose-5-phosphate.

Intracellular Metabolite Concentrations and Reaction Reversibilities—Although the above physiological and transcriptional data demonstrate malate to be one of two preferred carbon sources for *B. subtilis*, they do not reveal the intracellular fate of malate. To use ^{13}C-flux analysis for this purpose (11, 12), one requires knowledge on reaction reversibilities to simulate the distribution of ^{13}C-tracer atoms. Because this knowledge was not available for growth on malate or glucose plus malate, we developed a rigorous approach for deriving these reaction reversibilities that avoid error-prone, intuitive, and *ad hoc* decisions on reaction reversibilities (Fig. 1). In essence, the thermodynamic framework combines thermodynamic principles and *in vivo* intracellular metabolite concentrations to infer reaction reversibilities, as described under "Experimental Procedures."

Steady state intracellular concentrations of 41 metabolites were determined using GC-TOF (25) and liquid chromatography-MS/MS (26) analyses during exponential growth of *B. subtilis* on glucose, malate, and the mixture of glucose plus malate (Fig. 4 and supplemental Appendix B). Generally, absolute metabolite concentrations varied over 2–3 orders of magnitude with the S.D. for most compounds ranging from 10 to 30% (supplemental Appendix B). The concentration of the adenine nucleotides (*AxP*) and the redox cofactors NAD(H) and NADP(H) could only be determined as the combined pools. Based on NET analysis (17), all three datasets where thermodynamically consistent with the expected direction of fluxes. For glucose-grown cells, a further indicator for quenching efficiency is the ratio of glucose 6-phosphate to fructose 6-phosphate. This ratio quickly drops if glucose influx stops before metabolism is arrested or samples warm up before extraction. The ratio of glucose 6-phosphate and fructose 6-phosphate was found to be similar to previously reported values for rapidly quenched *Saccharomyces cerevisiae* (25).

When normalized to growth on glucose, malate metabolism leads to significantly lower metabolite concentrations in upper glycolysis and the pentose phosphate pathway and high concentration in lower glycolysis and TCA cycle. Although generally preserved, these changes were less pronounced during co-utilization of glucose and malate. The most pronounced concentration changes were observed for those metabolites that are closest to the entry point of the carbon source; *i.e.* hexose phosphates on glucose and

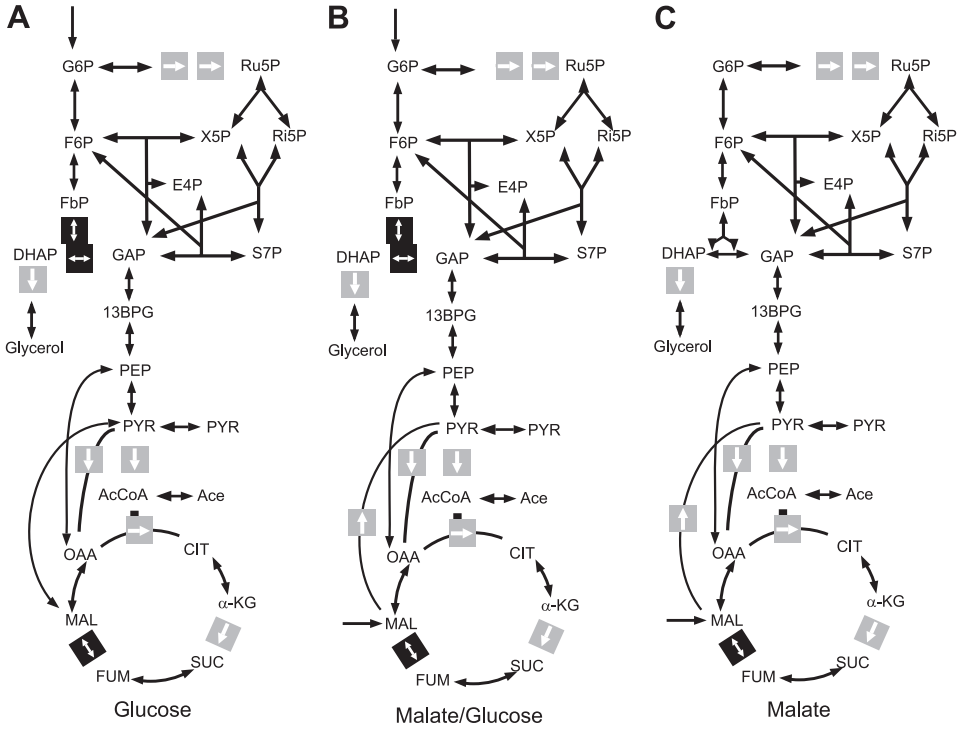

FIGURE 5. **Reaction reversibility constraints derived by thermodynamic analysis of steady state intracellular metabolite concentrations of *B. subtilis* during growth on glucose (*A*), glucose plus malate (*B*), and malate (*C*).** *Gray* and *black boxes* denote unidirectional and reversible reactions, respectively. All other reactions were considered to be freely reversible due to insufficient thermodynamic evidence. *13BPG*, 1,3-biphosphoglyceric acid; *Ace*, acetic acid; *α-KG*, 2-oxoglutaric acid; *CIT*, citrate; *DHAP*, dihydroxyacetone phosphate; *E4P*, erythrose 4-phosphate; *F6P*, fructose 6-phosphate; *FbP*, fructose 1,6-bisphosphate; *FUM*, fumaric acid; *G6P*, glucose 6-phosphate; *GAP*, glyceraldehyde 3-phosphate; *MAL*, malic acid; *OAA*, oxaloacetate; *PEP*, phosphoenolpyruvic acid; *Ri5P*, ribose 5-phosphate; *Ru5P*, ribulose 5-phosphate; *S7P*, sedoheptulose 7-phosphate; *X5P*, xylose 5-phosphate.

fumarate and succinate on malate. Because malate feeding primarily increases the concentration of the four-carbon organic acids and not the other TCA cycle intermediates, we have indirect evidence that the four-carbon branch and not the entire cycle is predominantly used.

Deriving Condition-specific Stoichiometric Networks—On the basis of the above-determined metabolite concentrations (supplemental Appendix B) we calculated *in vivo* Gibbs energies of reactions (supplemental Appendix C). All reactions in the initial network were considered to be freely reversible unless sufficient thermodynamic evidence was available based on the four criteria mentioned in Fig. 2. For growth on glucose, seven reactions could be defined as unidirectional and three as fully reversible, whereas insufficient information was available for the remaining 27 reactions. Overall the reaction reversibilities for the three substrate-specific stoichiometric networks were similar (Fig. 5). The most noteworthy difference was the reaction catalyzed by malic enzyme, which was unidirectional whenever malate was present but undefined in the glucose network. This is primarily caused by the high intracellular malate concentrations during growth on malate, thereby shifting the equilibrium of this reaction toward pyruvate.

The here-predicted reversibilities are generally in agreement with previously made modeling assumptions (16, 22, 36). Nevertheless, roughly two-thirds of the investigated reversibilities remain undefined. In these cases (i) either not all metabolites encompassing a reaction were quantified and, thus, make it impossible to resolve the reaction reversibility, or (ii) the metabolite measurements were not precise enough to reduce the range of feasible Gibbs energies of reaction and, thus, do not meet the postulated reversibility criteria (Fig. 2). Additional and more accurate measurements would, thus, be necessary to further increase the number of resolvable reversibilities. For the purpose of this work, however, the derived directionality constraints were sufficient.

^{13}C-Based Metabolic Flux Analysis—Equipped with a verified analytical model for ^{13}C-data interpretation, we next performed ^{13}C-labeling experiments in shake flask batch cultures with 20% [U-$^{13}C_4$]-malate, 20% [U-$^{13}C_6$]glucose, or a mixture of 20% [U-$^{13}C_4$]malate and 20% [U-$^{13}C_6$]glucose. Using whole isotopologue analysis, metabolic fluxes were estimated by iteratively fitting simulated ^{13}C-label distributions for a chosen set of metabolic fluxes to the measured ^{13}C-label distributions in proteinogenic amino acids, which provide analytical access to the carbon backbone of eight intermediates of central carbon metabolism (13).

The flux distribution during exponential growth on glucose (Fig. 6*A*) compares favorably to previously reported values for the same strain (22, 37). Glucose was primarily catabolized through glycolysis and then either secreted as acetate or combusted to CO_2 via the TCA cycle. Similar to previous studies (16, 38, 39), exchange fluxes for most reactions in the network cannot be accurately estimated because of the sparseness of the ^{13}C-labeling data from proteinogenic amino acids (supplemental Appendices A). The good correspondence between our and previously reported flux distributions adds to the credibility of deriving and using condition-specific network models.

During growth on malate, the incoming malate was converted to PEP and pyruvate, resulting in high gluconeogenic fluxes and overflow metabolism of pyruvate and acetate (Fig. 6*C*). Somewhat unexpectedly, only 10% of the malate was respired via the TCA cycle, whereas the majority was secreted as overflow metabolites. Glycolytic fluxes were reverted from PEP upwards for supplying biomass precursors originating from the pentose phosphate (PP) pathway and glycolysis. Co-utilization of glucose and malate also led to high gluconeogenic fluxes and overflow metabolism (Fig. 6*B*). The concomitant uptake of glucose, however, caused glycolytic fluxes to be directed downward toward PEP synthesis. The flux patterns during co-utilization, thus, resemble those of malate-feeding for the lower part and those of glucose-feeding for the upper part of central carbon metabolism.

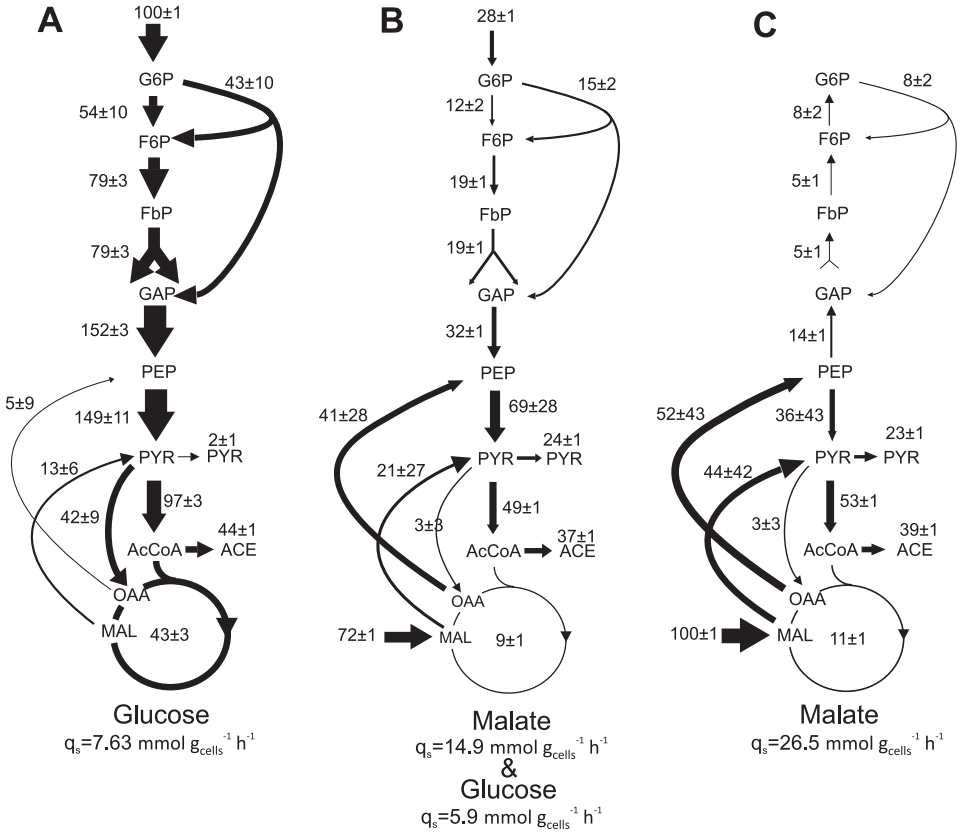

FIGURE 6. **Relative distributions of intracellular fluxes in *B. subtilis* grown on glucose (*A*), a mixture of glucose plus malate (*B*), and malate (*C*).** Fluxes were obtained by whole isotopologue analysis from GC-MS-detected ^{13}C patterns in proteinogenic amino acids and the physiological data (Table 2) combined with the substrate-specific metabolic network (Fig. 5). Labeling was achieved by growing cells on a mixture of 20% U-^{13}C carbon source and 80% naturally labeled carbon source. S.D. were obtained from Monte Carlo simulations. To facilitate cross-comparison, the absolute flux values (supplemental Appendix A) were normalized to the substrate uptakes, and these relative values are represented by *arrow size* and the *numerical value*. *ACE*, acetic acid; *F6P*, fructose 6-phosphate; *FbP*, fructose 1,6-bisphosphate; *G6P*, glucose-6-phosphate; *GAP*, glyceraldehyde 3-phosphate; *MAL*, malic acid; *OAA*, oxaloacetate; *PEP*, phosphoenolpyruvic acid; *α-KG*, 2-oxoglutaric acid; *CIT*, citrate; *FUM*, fumaric acid; *Ri5P*, ribose 5-phosphate; *Ru5P*, ribulose 5-phosphate; *GAP*, glyceraldehyde-3-phosphate.

Under either condition with malate, low relative fluxes through the PP pathway were estimated. To better understand the network-wide balancing of the biosynthetic reducing equivalent NADPH, we quantified the anabolic NADPH consumption from the known biochemical requirements of NADPH for macromolecules biosynthesis (16) (Fig. 7). On malate, NADPH was also consumed in the gluconeogenic reaction catalyzed by the NADPH-dependent glyceraldehyde-3-phosphate dehydrogenase (GapB) (40). The catabolic NADPH production was quantified from the carbon fluxes through the NADPH-producing reactions of the oxidative PP pathway, isocitrate dehydrogenase, and malic enzyme. *B. subtilis* contains four paralogous malic enzyme isoforms, the NADPH-producing isoenzyme YtsJ and the NADH-producing isoenzymes MaeA, MalN, and MleA (41); thus, the carbon flux through this reaction does not unequivocally reveal the concomitant NADPH production. From balancing the NADPH-consuming and -producing fluxes (Fig. 7), it is obvious that the catabolic NADPH production via the PP pathway and isocitrate dehydrogenase match the anabolic demands during growth on glucose as described before (22). In the presence of malate, however, these two sources of NADPH are insufficient such that about 40–50% of the anabolic NADPH demand must be supplied via the NADPH-dependent malic enzyme (Fig. 7). This view is consistent with an earlier knock-out study showing that YtsJ has the major physiological role in malate utilization, for which none of the other three malic enzymes could compensate (41).

Although the relative distribution of fluxes (Fig. 6) would suggest lower TCA cycle fluxes on malate, the absolute fluxes through the citrate synthase in the TCA cycle are rather similar on glucose (3.3 mmol g_{cells}^{-1} h^{-1}) and malate (2.8 mmol g_{cells}^{-1} h^{-1}). Because this flux is reduced to 1.7 mmol g_{cells}^{-1} h^{-1} on glucose plus malate, the two substrates have apparently a synergistic effect on TCA cycle, assuming that the absolute TCA cycle flux is a functional measure of repression (42). Until now, catabolite repression of TCA cycle-encoding genes was assumed to be exclusively elicited by glycolytic carbon sources (43). To verify this repressive effect genetically, the *in vivo* expression levels of the citrate synthase (CitZ) and the isocitrate dehydrogenase (Idh) genes for the three conditions were determined from tilling array data (Roche Applied Science). In line with our flux results, the expression level was significantly repressed during growth on malate plus glucose.[3]

Accuracy of the Estimated Flux Patterns—Because the reliability of flux analysis depends in part on the employed metabolic model, erroneous and missing reactions may lead to incorrect simulated ^{13}C-labeling patterns and, thus, incorrectly estimated fluxes. To ensure the accuracy of the estimated fluxes (Fig. 6), two tests were performed. First, we tested whether the estimated fluxes are statistically acceptable within the 95% confidence interval using the probability (*P*) (15, 16),

$$P\left(\chi^2 > \frac{SS}{n-p}\right) \qquad \text{(Eq. 6)}$$

Here *SS* is the minimal residual of squares, *n* is the number of independent data points, and *p* is the number of free parameters in the model. For all three conditions, statistically acceptable flux patterns where determined with $P(\chi^2 \dagger 1.88) = 0.17$, $P(\chi^2 \dagger 1.44) = 0.23$,

[3] S. Aymerich, personal communication.

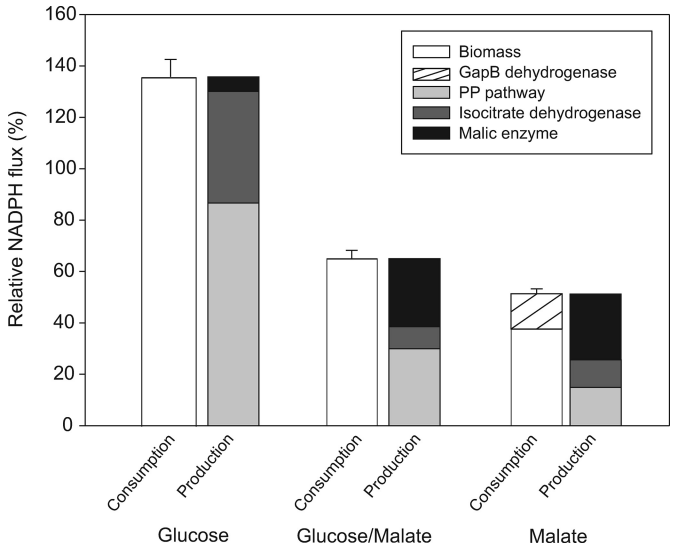

FIGURE 7. **Anabolic consumption and catabolic production of NADPH in *B. subtilis* grown on glucose, malate and a mixture of glucose plus malate.** The NADPH consumption was quantified from the known biochemical requirements of NADPH for growth dependent macromolecules biosynthesis (16). During growth on malate alone NADPH is also consumed via the NADPH-dependent glyceraldehyde-3-phosphate dehydrogenase (GapB). NADPH production was calculated from the fluxes for the NADPH-producing reactions catalyzed by the oxidative PP pathway enzymes, isocitrate dehydrogenase and malic enzyme (Fig. 6 and supplemental Appendix A). Because of the inability to distinguish between fluxes through the NADH and NADPH-producing malic enzyme, these values were calculated by balancing NADPH production and consumption.

and $P(\chi^2 \geq 1.00) = 0.32$ for the glucose, glucose plus malate, and malate cases, respectively.

Second, the S.D. for the metabolic fluxes were derived from Monte Carlo simulations (Fig. 6 and supplemental Appendix A) (44, 45). To mimic measurement errors, Gaussian noise was added to the measured ^{13}C-labeling data, and fluxes were re-estimated, thereby providing a measure for the sensitivity of the different fluxes. In general, most net fluxes could be accurately estimated with the exception of the gluconeogenic fluxes catalyzed by malic enzyme and PEP carboxykinase. Although their joint net flux is observable, their relative contributions are not fully resolvable in all cases with malate. This is because the isotopologue distribution of both enzyme substrates, malate (malic enzyme) and oxaloacetate (PEP carboxykinase), are in rapid equilibrium via the highly reversible malate dehydrogenase catalyzed reaction.

DISCUSSION

We demonstrate here that the gluconeogenic substrate malate is a preferred carbon source for *B. subtilis* because it (i) is unusually rapidly metabolized, (ii) has a maximal specific growth rate similar to that of glucose, (iii) is co-utilized with glucose, and (iv) represses the uptake of alternative carbon sources both at the transcriptional and physiological level. This differs from the commonly held view that *B. subtilis* first metabolizes PTS carbohydrates followed by non-PTS carbohydrate and, finally, organic acids (3, 5, 7, 8). Such a preference of gluconeogenic substrates over carbohydrates is also referred to as reverse catabolite repression (2) and found in *Pseudomonas aeruginosa* (46–48). Other examples are the Gram-negative bacterium *Rhizobium meliloti* (49) and the Gram-positive soil bacterium *Arthrobacter crystallopoietes* (50), both preferring succinate over glucose. *B. subtilis* appears to be unusual because it does not prefer one over the other but, instead, equally prefers a glycolytic and a gluconeogenic carbon source.

Why is malate a preferred substrate for *B. subtilis*? Generally it is taken for granted that glucose is preferred because of its abundance in plant material, but the vast majority of glucose must first be liberated from various polymers. Malate, in contrast, is an abundant free intermediate in plants, for example in almost all vacuoles, as the counter ion in stomata, and of course in many fruits such as apples. Possibly more important for *B. subtilis*, however, is the often substantial secretion of carboxylic acids, in particular malate, by plant roots into the rhizosphere (51). These carboxylic acids acidify the surrounding soil and can act as metal chelators to withstand toxic levels of heavy metals (52) or as phosphate solubilizers (53). Because carboxylic acids represent a common food source of soil dwelling microbes, plants achieve some control over their microbial root communities by such rhizodeposition that enables recruiting beneficial bacteria that help to fend off plant pathogens (53). Precisely this nutrient-based interaction has been shown for *B. subtilis* FB15, which is recruited as a beneficial rhizobacterium by *Arabidopsis thaliana* through secretion of large amounts of malate (54).

Mechanistically, it remains to be elucidated how malate represses the uptake of other carbon sources and why malate uptake is not repressed in the presence of glucose. According to the current model of the global carbon catabolite repression mechanism in *B. subtilis*, repression is brought about by the HPr kinase-catalyzed phosphorylation of HPr at its Ser-46 residue. This effect is propagated globally by the pleiotropic transcription factor CcpA (6). It is known that fructose 1,6-phosphate (FBP) is a main signal for CcpA-dependent catabolite repression and is, thus, a key signaling molecule for the regulation of the carbon metabolism in *B. subtilis* (43). At higher FBP concentrations, HPr kinase activity sharply increases and reaches a plateau at about 5 mM FBP (55). In our experiments we detected FBP levels of 6.2 and 7.6 mM during growth on glucose plus malate and glucose, respectively, that would be sufficient for a high HPr kinase activity. The intracellular FBP concentration on malate, in contrast, was only 1.5 mM, rendering it unlikely that FBP is the primary metabolic signal on malate.

A second gene encoding the HPr-like protein Crh was discovered in the genome (56). It shares 45% sequence identity with HPr and contains the regulatory serine but not the active histidine site. Recently, Warner and Lolkema (57) hypothesized that HPr and Crh may have carbon source-specific functions, with HPr-dependent repression predominating during growth on carbohydrates and Crh regulating carbon catabolite repression during growth on gluconeogenic carbon sources. In their growth experiments on succinate, glutamate, and citrate, they observed that repression of the citrate transporter (CitM) seemed to rely almost exclusively on Crh but not on HPr. Although not tested, it is tempting to speculate that malate might also act via Crh.

In conclusion, the varying concentrations for FBP under the three conditions, the possible role of Crh in malate utilization, and the differing degree and hierarchy of the repressive effect of glucose and malate provide evidence for different underlying mechanisms of carbon catabolite repression during growth on glucose and malate.

Acknowledgments—We thank Mark Fogg and Tony Wilkinson for constructing the pBaSysBioII derivative plasmids used in this study and Vincent Fromion for help with the fluorescence data analysis. We thank Dominik Heer and Inés Rodriguez-Alvarez for critical remarks on the manuscript.

REFERENCES

1. Jacob, F., and Monod, J. (1961) *J. Mol. Biol.* **3,** 318–356
2. Görke, B., and Stülke, J. (2008) *Nat. Rev. Microbiol.* **6,** 613–624
3. Brückner, R., and Titgemeyer, F. (2002) *FEMS Microbiol. Lett.* **209,** 141–148
4. Doan, T., Servant, P., Tojo, S., Yamaguchi, H., Lerondel, G., Yoshida, K., Fujita, Y., and Aymerich, S. (2003) *Microbiology* **149,** 2331–2343
5. Asai, K., Baik, S. H., Kasahara, Y., Moriya, S., and Ogasawara, N. (2000) *Microbiology* **146,** 263–271
6. Henkin, T. M., Grundy, F. J., Nicholson, W. L., and Chambliss, G. H. (1991) *Mol. Microbiol.* **5,** 575–584
7. Servant, P., Le Coq, D., and Aymerich, S. (2005) *Mol. Microbiol.* **55,** 1435–1451
8. Singh, K. D., Schmalisch, M. H., Stülke, J., and Görke, B. (2008) *J. Bacteriol.* **190,** 7275–7284
9. Warner, J. B., Krom, B. P., Magni, C., Konings, W. N., and Lolkema, J. S. (2000) *J. Bacteriol.* **182,** 6099–6105
10. Wei, Y., Guffanti, A. A., Ito, M., and Krulwich, T. A. (2000) *J. Biol. Chem.* **275,** 30287–30292
11. Sauer, U. (2006) *Mol. Syst. Biol.* **2,** 62
12. Wiechert, W. (2001) *Metab. Eng.* **3,** 195–206
13. Zamboni, N., Fendt, S. M., Rühl, M., and Sauer, U. (2009) *Nat. Protoc.* **4,** 878–892
14. Zhao, J., and Shimizu, K. (2003) *J. Biotechnol.* **101,** 101–117
15. van Winden, W. A., van Dam, J. C., Ras, C., Kleijn, R. J., Vinke, J. L., van Gulik, W. M., and Heijnen, J. J. (2005) *FEMS Yeast Res.* **5,** 559–568
16. Dauner, M., Bailey, J. E., and Sauer, U. (2001) *Biotechnol. Bioeng.* **76,** 144–156
17. Kummel, A., Panke, S., and Heinemann, M. (2006) *Mol. Syst. Biol.* **2,** 34
18. Zamboni, N., Kümmel, A., and Heinemann, M. (2008) *BMC Bioinformatics* **9,** 199
19. Wiechert, W. (2007) *Biophys. J.* **93,** 2255–2264
20. Jules, M., Le Chat, L., Aymerich, S., and Le Coq, D. (2009) *J. Bacteriol.* **191,** 3168–3171
21. Sauer, U., Lasko, D. R., Fiaux, J., Hochuli, M., Glaser, R., Szyperski, T., Wüthrich, K., and Bailey, J. E. (1999) *J. Bacteriol.* **181,** 6679–6688
22. Tännler, S., Decasper, S., and Sauer, U. (2008) *Microb. Cell Fact.* **7,** 19
23. Cormack, B. P., Valdivia, R. H., and Falkow, S. (1996) *Gene* **173,** 33–38
24. Bolten, C. J., Kiefer, P., Letisse, F., Portais, J. C., and Wittmann, C. (2007) *Anal. Chem* **79,** 3843–3849
25. Ewald, J. C., Heux, S., and Zamboni, N. (2009) *Anal. Chem.* **81,** 3623–3629
26. Büscher, J. M., Czernik, D., Ewald, J. C., Sauer, U., and Zamboni, N. (2009) *Anal. Chem.* **81,** 2135–2143
27. Alberty, R. A. (2003) *Thermodynamics of Biochemical Reactions*, John Wiley & Sons, Inc., New York
28. Oh, Y. K., Palsson, B. O., Park, S. M., Schilling, C. H., and Mahadevan, R. (2007) *J. Biol. Chem.* **282,** 28791–28799
29. Breeuwer, P., Drocourt, J., Rombouts, F. M., and Abee, T. (1996) *Appl. Environ. Microbiol.* **62,** 178–183
30. Voets, T., Droogmans, G., Raskin, G., Eggermont, J., and Nilius, B. (1999) *Proc. Natl. Acad. Sci. U.S.A.* **96,** 5298–5303
31. Beard, D. A., and Qian, H. (2007) *PLoS One* **2,** e144
32. Fischer, E., and Sauer, U. (2003) *Eur. J. Biochem.* **270,** 880–891
33. Kleijn, R. J., van Winden, W. A., van Gulik, W. M., and Heijnen, J. J. (2005) *FEBS J.* **272,** 4970–4982
34. Wiechert, W., Möllney, M., Isermann, N., Wurzel, M., and de Graaf, A. A. (1999) *Biotechnol. Bioeng.* **66,** 69–85
35. Fujita, Y. (2009) *Biosci. Biotechnol. Biochem.* **73,** 245–259
36. Fuhrer, T., Fischer, E., and Sauer, U. (2005) *J. Bacteriol.* **187,** 1581–1590
37. Fischer, E., and Sauer, U. (2005) *Nat. Genet.* **37,** 636–640
38. Gombert, A. K., Moreira dos Santos, M., Christensen, B., and Nielsen, J. (2001) *J. Bacteriol.* **183,** 1441–1451
39. Kleijn, R. J., Geertman, J. M., Nfor, B. K., Ras, C., Schipper, D., Pronk, J. T., Heijnen, J. J., van Maris, A. J., and van Winden, W. A. (2007) *FEMS Yeast Res.* **7,** 216–231
40. Fillinger, S., Boschi-Muller, S., Azza, S., Dervyn, E., Branlant, G., and Aymerich, S. (2000) *J. Biol. Chem.* **275,** 14031–14037
41. Lerondel, G., Doan, T., Zamboni, N., Sauer, U., and Aymerich, S. (2006) *J. Bacteriol.* **188,** 4727–4736
42. Schilling, O., Frick, O., Herzberg, C., Ehrenreich, A., Heinzle, E., Wittmann, C., and Stülke, J. (2007) *Appl. Environ. Microbiol.* **73,** 499–507
43. Aymerich, S., Goelzer, A., and Fromion, V. (2007) *Global Regulatory Networks in Bacillus subtilis*, pp. 39–73, Transworld Research Network, Kerala, India
44. Schmidt, K., Nielsen, J., and Villadsen, J. (1999) *J. Biotechnol.* **71,** 175–189
45. Möllney, M., Wiechert, W., Kownatzki, D., and de Graaf, A. A. (1999) *Biotechnol. Bioeng.* **66,** 86–103
46. Collier, D. N., Hager, P. W., and Phibbs, P. V., Jr. (1996) *Res. Microbiol.* **147,** 551–561
47. Siegel, L. S., Hylemon, P. B., and Phibbs, P. V., Jr. (1977) *J. Bacteriol.* **129,** 87–96
48. Wolff, J. A., MacGregor, C. H., Eisenberg, R. C., and Phibbs, P. V., Jr. (1991) *J. Bacteriol.* **173,** 4700–4706
49. Ucker, D. S., and Signer, E. R. (1978) *J. Bacteriol.* **136,** 1197–1200
50. Krulwich, T. A., and Ensign, J. C. (1969) *J. Bacteriol.* **97,** 526–534
51. Bais, H. P., Weir, T. L., Perry, L. G., Gilroy, S., and Vivanco, J. M. (2006) *Annu. Rev. Plant Biol.* **57,** 233–266
52. Liu, J., Magalhaes, J. V., Shaff, J., and Kochian, L. V. (2009) *Plant J.* **57,** 389–399
53. Weisskopf, L., Le Bayon, R. C., Kohler, F., Page, V., Jossi, M., Gobat, J. M., Martinoia, E., and Aragno, M. (2008) *Soil Biol. Biochem.* **40,** 1772–1780
54. Rudrappa, T., Czymmek, K. J., Paré, P. W., and Bais, H. P. (2008) *Plant Physiol.* **148,** 1547–1556
55. Jault, J. M., Fieulaine, S., Nessler, S., Gonzalo, P., Di Pietro, A., Deutscher, J., and Galinier, A. (2000) *J. Biol. Chem.* **275,** 1773–1780
56. Galinier, A., Haiech, J., Kilhoffer, M. C., Jaquinod, M., Stülke, J., Deutscher, J., and Martin-Verstraete, I. (1997) *Proc. Natl. Acad. Sci. U.S.A.* **94,** 8439–8444
57. Warner, J. B., and Lolkema, J. S. (2003) *FEMS Microbiol. Lett.* **220,** 277–280
58. Commichau, F. M., Wacker, I., Schleider, J., Blencke, H. M., Reif, I., Tripal, P., and Stülke, J. (2007) *J. Mol. Microbiol. Biotechnol.* **12,** 106–113